Enhanced Performance of Asymmetrically Clipped DC-Biased Optical OFDM Systems Using Adjacent Symbol Detection

Wei-Wen Hu, *Member, IEEE*

***Abstract*—Compared to the direct current (DC) biased optical OFDM (DCO-OFDM) and asymmetrically clipped optical orthogonal frequency division multiplexing (ACO-OFDM) schemes, the asymmetrically clipped DC biased optical OFDM (ADO-OFDM) has demonstrated a better balance between optical power efficiency and spectrum efficiency. However, both the traditional ADO-OFDM and ADO-OFDM with iteration receiver suffer from an error floor issue when a lower DC bias is allocated to the DCO-OFDM branch. In this paper, we propose an enhanced receiving technique for ADO-OFDM that introduces an adjacent symbol detection (ASD) scheme in the DCO-OFDM branch of ADO-OFDM, named as ASD-based ADO-OFDM (ASD-ADO-OFDM). Simulation results indicate that the proposed ASD-ADO-OFDM provides a lower bit error rate performance at lower DC bias and fewer computational complexity compared with traditional ADO-OFDM with iteration receiver.**

***Index Terms*—Direct current, ADO-OFDM, Hermitian symmetry, DCO-OFDM.**

I. Introduction

VISIBLE light communication (VLC) has demonstrated significant potential for indoor wireless communication due to its dual functions of illumination and communication [1]. In VLC systems, orthogonal frequency division multiplexing (OFDM) is the most commonly used multicarrier modulation scheme, offering resistance to inter-symbol interference and high spectral efficiency [2], [3], [4], [5], [6]. As the optical signal amplitude must be real and non-negative to drive light-emitting diodes, numerous unipolar signals for optical OFDM have been developed and can be divided into two major categories. The first category is the direct current (DC) biased method, in which a DC bias is superimposed with the bipolar signals of optical OFDM, known as DC biased optical OFDM (DCO-OFDM) [7], [8], [9], [10], [11], [12]. However, DCO-OFDM suffers from power inefficiency and a bit error rate (BER) plateau when the added DC bias value is too high or low, respectively. The second category is the clipping-based method, in which the operation of clipping at zero is added with the bipolar signals of optical OFDM, called asymmetrically clipped optical OFDM (ACO-OFDM) [13], [14], [15], [16], [17], [18] or pulse amplitude modulation discrete multitone (PAM-DMT) [19], [20], [21]. Although ACO-OFDM and PAM-DMT have higher power efficiency than DCO-OFDM, they introduce a half spectral efficiency because only odd subcarriers or the imaginary part of the subcarriers are used.

To achieve a better balance between spectral efficiency and power efficiency, an alternative method called asymmetrically clipped DC biased optical OFDM (ADO-OFDM) [22], [23], [24] was proposed. This method assigns odd subcarriers to ACO-OFDM symbols and even subcarriers to DCO-OFDM symbols, allowing for all subcarriers to be used for data transmission. ADO-OFDM possess the advantages of ACO-OFDM and DCO-OFDM because all subcarriers are adopted to transmit the data. However, traditional ADO-OFDM receiver, named as T-ADO-OFDM, suffers from clipping noise when the DC bias is lower, resulting in the error floor of BER [22]. On the other hand, the ADO-OFDM system with an iterative receiver, named as IT-ADO-OFDM, was proposed to improve the detection performance [25]. In [25], the ACO-OFDM and DCO-OFDM signals are estimated in the frequency domain and then reconstructed in the time domain for each iteration. The reconstructed signals are further subtracted from the received signals to eliminate the time-domain interference between ACO-OFDM and DCO-OFDM signals. The estimation performance is improved by increasing iteration number, which results in a higher computational complexity than T-ADO-OFDM. Moreover, the signals in DCO-OFDM branch still encounter the clipping distortion when the added DC bais is lower, which means that the BER performance is not significantly improved even using iteration.

To enhance the BER performance, this paper proposed a novel adjacent symbol detection (ASD) scheme in the DCO-OFDM branch of ADO-OFDM system, named as ASD-based ADO-OFDM (ASD-ADO-OFDM). In ASD-ADO-OFDM system, a standard ACO-OFDM receiver is firstly used to decode the ACO-OFDM symbols on the odd subcarriers and then the corresponding reconstructed ACO-OFDM signals are obtained. Then, the DCO-OFDM signals in the time domain are obtained by subtracting the reconstructed ACO-OFDM signals from the received signals. The resulting signals are pairwise averaged to eliminate the influence of the AWGN noise due to the symmetry property of DCO-OFDM signals. The next process involves N-point FFT and ASD operations. In the ASD operation, only

Manuscript received 12 July 2023; revised 8 September 2023; accepted 10 October 2023. Date of publication 13 October 2023; date of current version 23 October 2023. This work was support by the National Science and Technology Council, Taiwan, under Grant NSTC 112-2221-E-150-019.

The author is with the Department of Electrical Engineering, National Formosa University, Yunlin 632, Taiwan (e-mail: huweiwen1106@gmail.com).

Digital Object Identifier 10.1109/JPHOT.2023.3324368

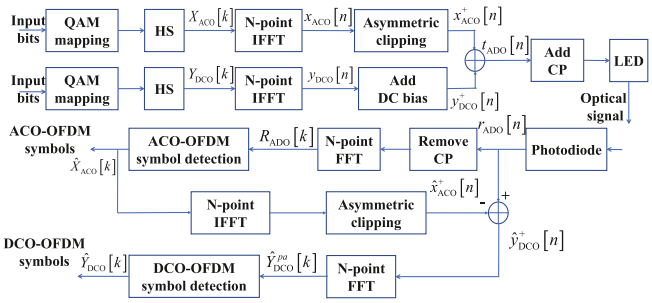

Fig. 1. Block diagram of the transmitter and receiver for T-ADO-OFDM system.

adjacent constellation symbols are considered when decoding DCO-OFDM symbols, rather than the entire constellation symbols, which avoids additional processing complexity in the IT-ADO-OFDM. It is demonstrated that the ASD-ADO-OFDM could provide a lower bit error rate performance at lower DC bias.

The remainder of the paper is structured as follows: Section II presents the system model of traditional ADO-OFDM system, while in Section III, the proposed ASD-ADO-OFDM system is described. In Section IV, the computational complexity of the ASD-ADO-OFDM receiver is compared to T-ADO-OFDM and IT-ADO-OFDM, while the corresponding BER performance of different methods are drawn in Section IV. Finally, Section V summarizes and concludes the paper.

II. The System Model of T-ADO-OFDM and IT-ADO-OFDM

In this section, the system models of the T-ADO-OFDM and IT-ADO-OFDM are briefly demonstrated. As shown in Fig. 1, two input random bit streams are generated and converted into QAM modulation symbols separately. Because T-ADO-OFDM transmitter assigns odd subcarriers and even subcarriers to ACO-OFDM symbols and DCO-OFDM symbols, respectively, the frequency-domain ACO-OFDM signals after applying the Hermitian symmetry can be written as [22]

$$X_{\mathrm{ACO}}[k]=\begin{cases} X[k], & k=1,3,\cdots,N/2-1 \\ X^{*}[N-k], & k=N/2+1,\cdots,N-1 \\ 0, & \text{otherwise} \end{cases} \tag{1}$$

where $(\cdot)^{*}$ is the operation of complex conjugation and $X[k]$ denotes the kth complex-valued QAM symbols with constellation size of M_o. Applying N-point IFFT operation on (1), the ACO-OFDM signals in the time domain can be obtained as [22]

$$x_{\mathrm{ACO}}[n]=\frac{1}{\sqrt{N}}\sum_{k=0}^{N-1}X_{\mathrm{ACO}}[k]\exp\left[\frac{j2\pi kn}{N}\right],0\le n\le N-1 \tag{2}$$

The $x_{\mathrm{ACO}}[n]$ has been proved to have antisymmetry property as follows [23]

$$x_{\mathrm{ACO}}[n]=-x_{\mathrm{ACO}}[n+N/2],0\le n\le N/2-1. \tag{3}$$

The unipolar ACO-OFDM signals are obtained by asymmetric clipping operation, indicating that the bipolar signals are simply clipped at zero as [22]

$$x_{\mathrm{ACO}}^{+}[n]=\begin{cases} x_{\mathrm{ACO}}[n], & x_{\mathrm{ACO}}[n]\ge 0 \\ 0, & x_{\mathrm{ACO}}[n]<0 \end{cases} \tag{4}$$

On the other hand, the frequency-domain DCO-OFDM signals after applying the Hermitian symmetry can be denoted as [22]

$$Y_{\mathrm{DCO}}[k]=\begin{cases} Y[k], & k=0,2,\cdots,N/2-2 \\ Y^{*}[N-k], & k=N/2+2,\cdots,N-2 \\ 0, & \text{otherwise} \end{cases} \tag{5}$$

where $Y[k]$ denotes the kth complex-valued QAM symbols with constellation size of M_e. Applying N-point IFFT operation on (5), the DCO-OFDM signals in the time domain can be obtained as [22]

$$y_{\mathrm{DCO}}[n]=\frac{1}{\sqrt{N}}\sum_{k=0}^{N-1}Y_{\mathrm{DCO}}[k]\exp\left[\frac{j2\pi kn}{N}\right],0\le n\le N-1 \tag{6}$$

The $y_{\mathrm{DCO}}[n]$ has been proved to have symmetry property as follows [23]

$$y_{\mathrm{DCO}}[n]=y_{\mathrm{DCO}}[n+N/2],0\le n\le N/2-1. \tag{7}$$

Unlike ACO-OFDM, the unipolar DCO-OFDM signals are obtained by adding a DC bias $B_{DC}=u\sqrt{E[|y_{DCO}[n]|^2]}=u\sigma_y$ to (6), where u is the clipping factor and σ_y is the standard deviation of $y_{\mathrm{DCO}}[n]$. The bias level in dB is defined as $10\log_{10}(u^2+1)$. Therefore, the unipolar DCO-OFDM signals are given by [23]

$$y_{\mathrm{DCO}}^{+}[n]=y_{\mathrm{DCO}}[n]+B_{DC} \tag{8}$$

Combining ACO-OFDM signals with DCO-OFDM signals, the transmitted ADO-OFDM signals can be formulated by [22]

$$t_{ADO}[n]=x_{\mathrm{ACO}}^{+}[n]+y_{\mathrm{DCO}}^{+}[n] \tag{9}$$

Finally, the signals with a cyclic prefix (CP) added to (9) are further processed by a digital-to-analog converter to drive a LED, which produces optical signals. Considering the LED nonlinearity, the ADO-OFDM signal can be expressed as [22]

$$t_{ADO}^{clip}[n]=\begin{cases} \varepsilon_{\mathrm{upper}}, & t_{ADO}[n]>\varepsilon_{\mathrm{upper}}, \\ t_{ADO}[n], & 0\le t_{ADO}[n]\le\varepsilon_{\mathrm{upper}}, \\ 0, & t_{ADO}[n]<0, \end{cases} \tag{10}$$

where $\varepsilon_{\mathrm{upper}}$ denotes the maximum permissible voltage.

At the receiver side, the received optical signal is firstly converted into the electrical signal using a photodiode. The received electrical signal can be expressed as [22]

$$r_{ADO}[n]=t_{ADO}^{clip}[n]\otimes h[n]+w[n], \tag{11}$$

where $\otimes$ denotes the circular convolution, $w[n]$ is AWGN noise and $h[n]$ denotes the channel impulse response. Then, $r_{ADO}[n]$ pass through the process of removing the cyclic prefix and N-point FFT operation. The resultant ACO-OFDM symbols on odd subcarriers can be estimated by conventional ACO-OFDM receiver. After that, time-domain ACO-OFDM signals can be

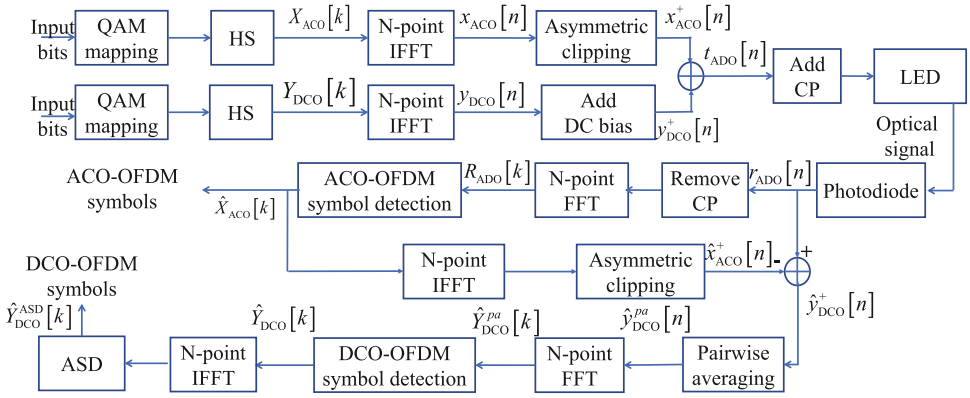

Fig. 2. Block diagram of the proposed transmitter and receiver for the ASD-ADO-OFDM systems.

regenerated and subtracted from the received signals. The DCO-OFDM symbols from even subcarriers could be estimated after the interference cancellation procedure [22]. As given by (8), when the added DC bias is too small, the significant clipping distortion occurs leading to severe detection errors. However, adding a higher DC bias is power inefficient. On the other hand, IT-ADO-OFDM has the same transmitter as that of T-ADO-OFDM. In the receiver of IT-ADO-OFDM, the ACO-OFDM and DCO-OFDM signals are detected in the frequency domain and then reconstructed in the time domain for each iteration. In this manner, the interference between ACO-OFDM and DCO-OFDM signals in the time domain could be eliminated by subtracting the reconstructed signals from the received signals. For the subsequent iteration, the same operation is performed iteratively until the maximum iteration number is reached [25]. Because T-ADO-OFDM and IT-ADO-OFDM have the similar receiver structure except for the iteration operations, the corresponding mathematical expressions of the receiver will be demonstrated in the following section for the sake of brevity.

III. The System Model of ASD-ADO-OFDM

In order to improve the performance of ADO-OFDM systems at the case of lower DC bias, this paper proposed an adjacent symbol detection scheme for ADO-OFDM systems, named as ASD-based ADO-OFDM (ASD-ADO-OFDM). Fig. 2 depicts the block diagram of the transmitter and receiver for the proposed ASD-ADO-OFDM systems. As shown in Fig. 2, the transmitter of the ASD-ADO-OFDM is equal to that of the T-ADO-OFDM and IT-ADO-OFDM. Therefore, the detection of the ACO-OFDM symbols on the odd subcarriers could be firstly estimated by using maximum likelihood (ML) detection as follows [25]

$$\hat{X}_{ACO}[k] = \underset{X_{ACO}[k]\in M_o}{\arg\min} \|X_{ACO}[k] - 2R_{ADO}[k]/H[k]\|^2, \tag{12}$$

where $k = 1, 3, \ldots N/2-1$, $\|\cdot\|$ is the Euclidean distance, $H[k]$ represents the channel frequency response, and $R_{ADO}[k]$ is the received frequency-domain signal obtained by N-point FFT operation as follows [25]

$$R_{ADO}[k] = T_{ADO}[k]H[k] + W[k], 0 \le k \le N-1 \tag{13}$$

In (13), $T_{ADO}[k]$ and $W[k]$ denote the frequency-domain signal of $t_{ADO}[n]$ and AWGN noise, respectively. The detection process of DCO-OFDM symbols in ASD-ADO-OFDM is demonstrated as follows. Firstly, the regenerated ACO-OFDM signals $\hat{x}^+_{ACO}[n]$ in the time domain can be obtained using N-point IFFT and asymmetric clipping operations as given by (2) and (4). The regenerated signals $\hat{x}^+_{ACO}[n]$ is subtracted from the $r_{ADO}[n]$ leading to DCO-OFDM signal $\hat{y}^+_{\mathrm{DCO}}[n]$ is given by

$$\begin{aligned}\hat{y}^+_{\mathrm{DCO}}[n] &= r_{\mathrm{ADO}}[n] - \hat{x}^+_{\mathrm{ACO}}[n] \\ &= y^+_{\mathrm{DCO}}[n] + x^+_{\mathrm{ACO}}[n] - \hat{x}^+_{\mathrm{ACO}}[n] + w[n] \\ &= y_{\mathrm{DCO}}[n] + B_{DC} + \underbrace{x^+_{\mathrm{ACO}}[n] - \hat{x}^+_{\mathrm{ACO}}[n]}_{e_{\mathrm{ACO}}[n]} + w[n]\end{aligned} \tag{14}$$

where $e_{\mathrm{ACO}}[n]$ represents the estimation error of ACO-OFDM symbol. After that, considering the symmetric property of time-domain DCO-OFDM signals, pairwise averaging could be used to decrease the influence of AWGN noise. On the basis of pairwise averaging, the resultant DCO-OFDM signal is expressed as

$$\begin{aligned}\hat{y}^{pa}_{\mathrm{DCO}}[n] &= \hat{y}^{pa}_{\mathrm{DCO}}[n + N/2] \\ &= \frac{1}{2}(\hat{y}^+_{\mathrm{DCO}}[n] + \hat{y}^+_{\mathrm{DCO}}[n + N/2])\end{aligned} \tag{15}$$

where $n = 0, 1, 2 \ldots, N/2-1$. Subsequently, the $\hat{y}^{pa}_{\mathrm{DCO}}[n]$ is fed into N-point FFT to obtain frequency-domain DCO-OFDM signals $\hat{Y}^{pa}_{\mathrm{DCO}}[k]$ as follows

$$\hat{Y}^{pa}_{\mathrm{DCO}}[k] = Y_{DCO}[k] + B_{DC} + E_{ACO}[k] + W[k] \tag{16}$$

where $E_{ACO}[k]$ denotes the frequency-domain component of $e_{ACO}[n]$

In T-ADO-OFDM systems, the DCO-OFDM symbols could be recovered applying ML detection on $\hat{Y}^{pa}_{\mathrm{DCO}}[k]$ as follows

$$\hat{Y}_{DCO}[k] = \underset{Y_{DCO}[k]\in M_e}{\arg\min} \|\hat{Y}^{pa}_{\mathrm{DCO}}[k] - Y_{DCO}[k]\|^2, \tag{17}$$

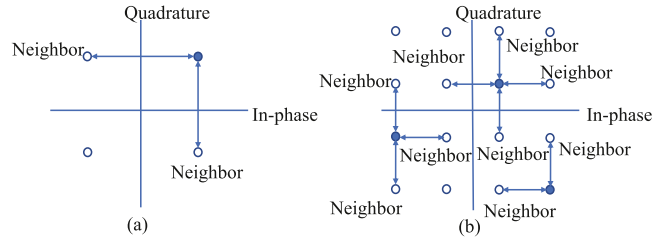

Fig. 3. Neighbor constellation points of (a) QPSK and (b) 16-QAM.

where $k = 2, 4, \ldots, N/2-2$. In the receiver of IT-ADO-OFDM, the ACO-OFDM and DCO-OFDM signals are detected in the frequency domain and then reconstructed in the time domain for each iteration. In this manner, (12) is used for generating the time-domain ACO-OFDM signals using from (1) to (4) and (17) is used for generating the time-domain DCO-OFDM signals using from (5) to (8).

At the initialization step of the ASD-ADO-OFDM, the detection process of ACO-OFDM symbol and DCO-OFDM symbol is the same as that of T-ADO-OFDM and IT-ADO-OFDM. With the introduction of iteration in ASD-ADO-OFDM, we adopt two strategies to decrease the computation complexity of iteration operation while maintaining the acceptable performance. Firstly, ASD-ADO-OFDM only considers the adjacent constellation symbols rather than whole constellation symbols when decoding DCO-OFDM symbols. The adjacent constellation symbols adopted in ASD-ADO-OFDM define the neighborhood symbols with the same Euclidean distance and given by Fig. 3. As seen in Fig. 3, each constellation point of QPSK has two neighbors with the same Euclidean distance while the number of neighbor for each constellation point of 16-QAM could be 2, 3, and 4. Secondly, the iteration of ASD-ADO-OFDM is only adopted in ASD block diagram of Fig. 2, which means that the entire reconstruction process of ACO-OFDM signal and DCO-OFDM signal are not considered in ASD-ADO-OFDM. Thus, the algorithm of the ASD block diagram within ASD-ADO-OFDM system is provided as follows. Step 1 is executed once for initialization, followed by the execution of steps 2 to 4 J times for each DCO-OFDM symbol.

Step 1: Set the iterator $j = 0$. The original frequency-domain DCO-OFDM symbols $\hat{Y}_{DCO}^{(0)}[k]$ are firstly estimated using (17), where the superscript of $\hat{Y}_{DCO}^{(0)}[k]$ is introduced to denote the initialization step of the ASD-ADO-OFDM receiver. Then the time-domain DCO-OFDM signals $\hat{y}_{\mathrm{DCO}}^{(0)}[n]$ could be reconstructed by imposing Hermitian symmetry and N-point IFFT on $\hat{Y}_{DCO}^{(0)}[k]$, which is given by

$$\hat{y}_{\mathrm{DCO}}^{(0)}[n] = \frac{1}{\sqrt{N}} \sum_{k=0}^{N-1} \hat{Y}_{DCO}^{(0)}[k] \exp\left[\frac{j2\pi kn}{N}\right], 0 \le n \le N-1 \tag{18}$$

Meanwhile, we define the metric as the difference between the $\hat{y}_{\mathrm{DCO}}^{+}[n]$ and $\hat{y}_{\mathrm{DCO}}^{(0)}[n]$, which is given by

$$Metric^{(0)} = \| \hat{y}_{\mathrm{DCO}}^{+}[n] - \hat{y}_{\mathrm{DCO}}^{(0)}[n] \|^2 \tag{19}$$

where $\hat{y}_{\mathrm{DCO}}^{+}[n]$ is obtained by (14).

Step 2: The estimated DCO-OFDM symbols $\hat{Y}_{DCO}^{(0)}[k]$ at first step are inputted to ASD block to update DCO-OFDM symbols. The operations of ASD block are described as follows. The symbol at the kth subcarrier, $\hat{Y}_{DCO}^{(0)}[k]$, is updated by substituting the estimated symbol with its l-th neighborhood constellation $\hat{Y}_{DCO}^{(0),l}[k]$ and fix other even subcarriers. The associated time-domain DCO-OFDM signals can be reconstructed to calculate the new metric in (19). The neighborhood constellation with the lowest metric is selected as the candidate for updating the symbol at the next even subcarrier. Because only one subcarrier is changed among whole subcarriers, instead of using Hermitian symmetry and N-point IFFT, the associated nth time-domain DCO-OFDM elements for each new $\hat{Y}_{DCO}^{(0),l}[k]$ could be reconstructed by the following equation,

$$\begin{aligned}\hat{y}_{\mathrm{DCO}}^{(0),l}[n] &= \frac{1}{\sqrt{N}} \hat{Y}_{DCO}^{(0),l}[k] \exp\left[\frac{j2\pi kn}{N}\right] \\ &+ \frac{1}{\sqrt{N}} \sum_{\substack{k'=0 \\ k' \neq k}}^{N-1} \hat{Y}_{DCO}^{(0)}[k'] \exp\left[\frac{j2\pi k'n}{N}\right],\end{aligned} \tag{20}$$

where $0 \le n \le N-1$. Noted that the second term of (20) is unchanged indicating that we could calculate once at the initialization step and store the values in the memory. Then the metrics of all L neighborhood constellations could be computed according to (19), where the symbol $\hat{Y}_{DCO}^{(0),l}[k]$ with the lowest metric is chosen as the candidates for updating the other even subcarriers as given by

$$\begin{aligned}\hat{Y}_{DCO}^{(0)}[k] &= \arg\min_{0 \le m \le L} Metric^{(0),l} \\ &= \arg\min_{0 \le l \le L} \| \hat{y}_{\mathrm{DCO}}^{+}[n] - \hat{y}_{\mathrm{DCO}}^{(0),l}[n] \|^2\end{aligned} \tag{21}$$

Step 3: Update $k = k + 2$. If $k < N/2 - 2$, return to step 2; otherwise, go to the next step.

Step 4: Update $j = j + 1$. If $j < J$, return to step 2; otherwise, terminate the iteration.

IV. The Analysis of Computational Complexity

In this section, we compare the computational complexity of the ASD-ADO-OFDM with the T-ADO-OFDM and the IT-ADO-OFDM. As can be seen in Figs. 1 and 2, all methods have the identical transmitter structures which result in the same computational complexity. Thus, the computational complexities are mainly determined by the receiver operations. Specifically, the overall computational complexities of all receivers in this paper is defined as the required number of computations of the Euclidean distance and IFFT/FFT blocks. As demonstrated in Fig. 1, the T-ADO-OFDM receiver requires two N-point FFT blocks and with one N-point IFFT block, where each N-point IFFT/FFT block has the computational complexity of $O(N \log_2 N)$. Moreover, the symbol detection of ACO-OFDM and DCO-OFDM requires computational complexity of Euclidean distance $O(M_o N/4)$ and $O(M_e N/4)$, respectively. Without loss of generality, the identical modulation

TABLE I
CCR COMPARISON FOR DIFFERENT PARAMETERS CONFIGURATIONS ($M = 16$)

		N=64	N=128	N=256	N=512
J=1	L=4	0.4844	0.4861	0.4875	0.4886
	L=2	0.4922	0.4931	0.4938	0.4943
J=2	L=4	0.6458	0.6481	0.6500	0.6515
	L=2	0.6562	0.6574	0.6583	0.6591
J=3	L=4	0.7266	0.7292	0.7312	0.7330
	L=2	0.7383	0.7396	0.7406	0.7415

are adopted in both ACO-OFDM branch and DCO-OFDM branch (i.e. $M_o = M_e = M$), the computational complexity of T-ADO-OFDM is expressed as

$$\begin{aligned} &C_{\text{T-ADO-OFDM}} \\ &= 3O(N\log_2 N) + O(M_oN/4) + O(M_eN/4) \\ &= 3O(N\log_2 N) + 2O(MN/4) \end{aligned} \tag{22}$$

Similarly, the computational complexity of IT-ADO-OFDM can be given by

$$\begin{aligned} &C_{\text{IT-ADO-OFDM}} \\ &= J[4O(N\log_2 N) + O(M_oN/4) + O(M_eN/4)] \\ &= J[4O(N\log_2 N) + 2O(MN/4)] \end{aligned} \tag{23}$$

where J is the number of iteration. Note that IT-ADO-OFDM receiver requires a additional IFFT block to regenerate the time-domain DCO-OFDM signals compared with T-ADO-OFDM receiver.

For the receiver of ASD-ADO-OFDM, the computational complexity of initialization step is the same as that of IT-ADO-OFDM receiver, where one N-point FFT block and one N-point IFFT block are needed for processing ACO-OFDM and DCO-OFDM signal detection and reconstruction, respectively. For the subsequent iteration, ASD-ADO-OFDM considers the adjacent constellation symbols rather than whole constellation symbols when decoding DCO-OFDM symbols. Therefore, the computational complexity of ASD-ADO-OFDM is expressed as

$$\begin{aligned} &C_{\text{ASD-ADO-OFDM}} \\ &= 4O(N\log_2 N) + O(M_oN/4) + O(M_eN/4) + JO(LN/4) \\ &= 4O(N\log_2 N) + 2O(MN/4) + JO(LN/4) \end{aligned} \tag{24}$$

In order to measure the improvement on the complexity, we define complexity reduction ratio (CRR) as follows

$$CRR = 1 - \frac{C_{\text{ASD-ADO-OFDM}}}{C_{\text{IT-ADO-OFDM}}} \tag{25}$$

The CCR comparison for different parameters configurations is summarized in Table I. It is found that the CCR is substantially reduced compared to the IT-ADO-OFDM system.

V. SIMULATION RESULTS

In this section, we present a comparison of the overall average BER performance of ASD-ADO-OFDM, T-ADO-OFDM, and IT-ADO-OFDM by MATLAB software. All systems employ an IFFT/FFT size of $N = 128$ and a cyclic prefix length of 16. To ensure a fair comparison, we assume equal optical power allocation between the DCO-OFDM branch and the ACO-OFDM branch for all systems [26]. Additionally, perfect symbol synchronization and channel estimation are assumed at the receiver side. Because the transmitter architecture of the proposed system is equal to that of traditional ADO-OFDM and ADO-OFDM with iterative receiver, we could assume that optical powers of the transmission signals are the same for all systems. Without loss of generality, the transmission optical power is set to unity. It is worth noting that we adopt identical modulation in both the ACO-OFDM branch and the DCO-OFDM branch (i.e. $M_o = M_e$).

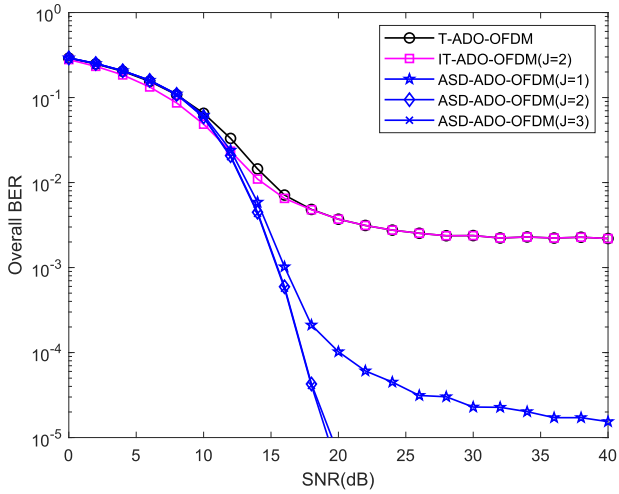

Fig. 4. Overall average BER performance comparison between T-ADO-OFDM, IT-ADO-OFDM, and ASD-ADO-OFDM ($B_{DC} = 1$ dB, QPSK).

A. Ideal LED Transmission

In this subsection, we first investigate BER performance comparisons between ASD-ADO-OFDM, T-ADO-OFDM and IT-ADO-OFDM with ideal LED transmission, which means the upper clipping level $\varepsilon_{\text{upper}}$ is infinite. For QPSK modulations, the simulations results regarding all systems with $B_{DC} = 1$ dB are provided in Fig. 4. It can be seen that T-ADO-OFDM exhibits the BER error floor for the lower DC bias. Although IT-ADO-OFDM has the lower BER in the range of SNR about 0 to 16 dB, IT-ADO-OFDM cannot improve the BER performance by increasing SNR, which is similar to the case in T-ADO-OFDM. This is because the clipping distortions in both T-ADO-OFDM and IT-ADO-OFDM are not removed completely when decoding DCO-OFDM symbols. As shown in Fig. 4, the proposed ASD-ADO-OFDM system significantly improves the BER performance in case of lower DC bias after the first iteration. However, the BER improvement is marginal when the number of iteration $J \geq 3$. Most importantly, we can lower the BER plateau level for T-ADO-OFDM and IT-ADO-OFDM by increasing B_{DC} value as shown in Fig. 5. In this case, ASD-ADO-OFDM provides the BER plateau free after first iteration. The high-order modulation 16-QAM are further investigated in Fig. 6, where $B_{DC} = 3$ dB is assumed for all

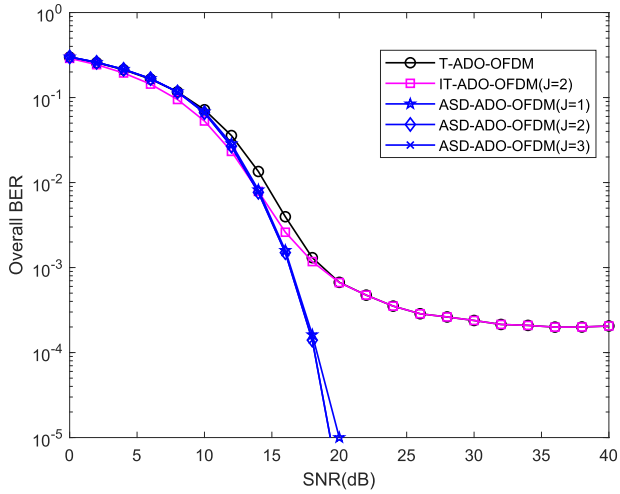

Fig. 5. Overall average BER performance comparison between T-ADO-OFDM, IT-ADO-OFDM, and ASD-ADO-OFDM ($B_{DC} = 2$ dB, QPSK).

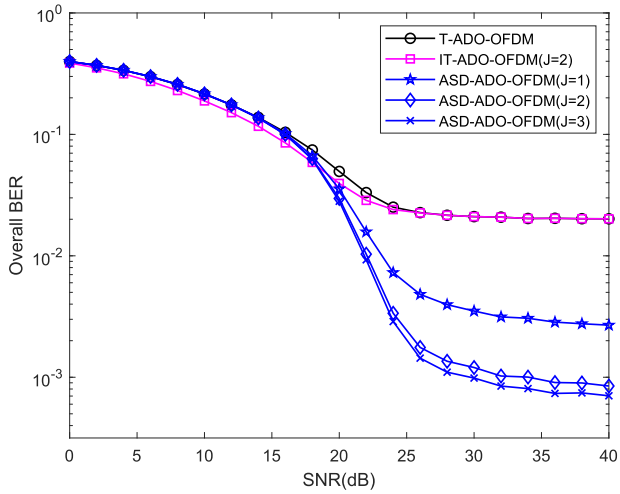

Fig. 6. Overall average BER performance comparison between T-ADO-OFDM, IT-ADO-OFDM, and ASD-ADO-OFDM ($B_{DC} = 3$ dB, 16-QAM).

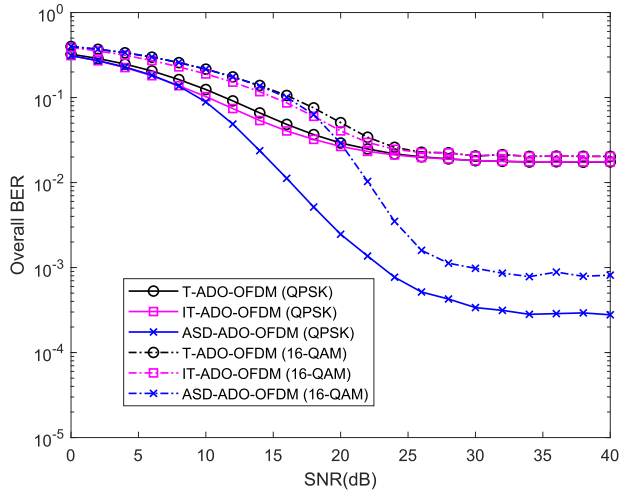

Fig. 7. Overall average BER performance comparison between T-ADO-OFDM, IT-ADO-OFDM, and ASD-ADO-OFDM ($B_{DC} = 2$ dB for QPSK and $B_{DC} = 3$ dB for 16-QAM).

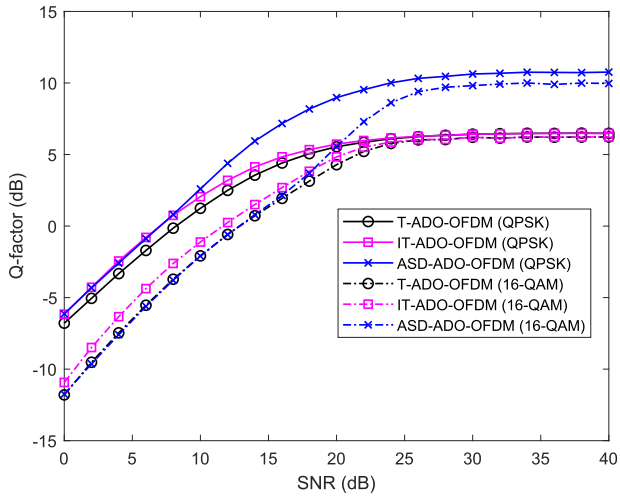

Fig. 8. Q-factor comparison between T-ADO-OFDM, IT-ADO-OFDM, and ASD-ADO-OFDM ($B_{DC} = 2$ dB for QPSK and $B_{DC} = 3$ dB for 16-QAM).

systems. As seen in Fig. 6, T-ADO-OFDM and IT-ADO-OFDM still cannot improve the BER performance significantly, while ASD-ADO-OFDM has a much lower error floor than that of T-ADO-OFDM and IT-ADO-OFDM.

B. Nonlinear LED Transmission

In order to meet the actual LED transmission, two upper clipping level $\varepsilon_{\text{upper}} = 2$ and $\varepsilon_{\text{upper}} = 4$ for QPSK and 16-QAM modulations are considered to determine the effects of LED nonlinearity on average BER performance as illustrated in Fig. 7. In this figure, the adopted B_{DC} values for QPSK and 16-QAM modulations are 2 dB and 3 dB, respectively. The number of iterations for IT-ADO-OFDM and ASD-ADO-OFDM is set to two. It can be seen that under the nonlinear LED transmission, the BER plateau level of T-ADO-OFDM and IT-ADO-OFDM is increased compared with the case of ideal LED transmission. Moreover, ASD-ADO-OFDM still improves the BER performance significantly for the lower DC bias.

C. Q-Factor

In this section, we further investigate the Q factor comparisons between ASD-ADO-OFDM, T-ADO-OFDM and IT-ADO-OFDM with nonlinear LED transmission. Generally, the relationship of Q-factor to BER is given by [27]

$$BER = \frac{1}{2} erfc\left(\frac{Q}{\sqrt{2}}\right) \tag{26}$$

where $erfc(\cdot)$ is the complementary error function defined by

$$erfc(x) = \frac{2}{\sqrt{\pi}} \int_x^{\pi} e^{-t^2} dt \tag{27}$$

Combining (26) and (27), the Q-factor in terms of dB could be calculated by substituting the obtained BER performance into following equation

$$Q(dB) = 20 \cdot \log_{10}\left(\sqrt{2} \cdot erfc^{-1}(2 \cdot BER)\right) \tag{28}$$

where $erfc^{-1}(\cdot)$ is the inverse function of $erfc(\cdot)$. The simulated Q-factor for all systems is shown in Fig. 8, where the simulation parameters for all systems are equal to that of Fig. 7. We can observe that ASD-ADO-OFDM has the higher Q-factor compared with the other two methods. Besides, the Q-factor improves as SNR increases, due to the fact that the higher SNR, the better BER performance.

VI. Conclusion

In this paper, we propose a novel adjacent symbol detection (ASD) scheme that can be applied to the DCO-OFDM branch of the ADO-OFDM system. The ASD scheme takes into account the distribution characteristic of clipping noise and only considers adjacent constellation symbols instead of the entire set of constellation symbols when decoding DCO-OFDM symbols. Simulation results show that the ASD-ADO-OFDM system can improve the BER performance significantly at case of lower DC bias. Moreover, we can observe that ASD-ADO-OFDM has the higher Q-factor compared with the T-ADO-OFDM and IT-ADO-OFDM systems.

References

[1] P. H. Pathak, X. Feng, P. Hu, and P. Mohapatra, "Visible light communication, networking, and sensing: A survey, potential and challenges," *IEEE Commun. Surveys Tut.*, vol. 17, no. 4, pp. 2047–2077, Fourthquarter 2015.

[2] X. Li, J. Huang, Y. Lyu, R. Ni, J. Luo, and J. Zhang, "Two types of mixed orthogonal frequency division multiplexing (X-OFDM) waveforms for optical wireless communications," *IEEE Trans. Wireless Commu.*, vol. 21, no. 2, pp. 1092–1102, Feb. 2022.

[3] Y. C. Chi, Y. C. Li, H. Y. Wang, P. Chun Peng, H. H. Lu, and G. R. Lin, "Optical 16-QAM-52-OFDM transmission at 4 Gbit/s by directly modulating a coherently injection-locked colorless laser diode," *Opt. Exp.*, vol. 20, no. 18, pp. 20071–20077, Aug. 2012.

[4] C. Y. Chen, P. Y. Wu, H. H. Lu, Y. P. Lin, J. Y. Wen, and F. C. Hu, "Bidirectional 16-QAM OFDM in-building network over SMF and free-space VLC transport," *Opt. Lett.*, vol. 38, no. 13, pp. 2345–2347, Jul. 2013.

[5] K. Mallick et al., "Bidirectional OFDM based MMW/THzW over fiber system for next generation communication," *IEEE Photon. J.*, vol. 13, no. 4, Aug. 2021, Art. no. 7301207.

[6] K. Mallick et al., "Cyclic prefix length optimization in OFDM-MMWOF/PAM4-FSO integrated system for future generation smart wireless communication," *Opt. Quantum Electron.*, vol. 55, no. 1, Jan. 2023, Art. no. 64.

[7] J. B. Carruthers and J. M. Kahn, "Multiple-subcarrier modulation for non-directed wireless infrared communication," *IEEE J. Sel. Areas Commun.*, vol. 14, no. 3, pp. 538–546, Apr. 1996.

[8] Y. Jiang, D. Sun, X. Zhu, T. Zhou, T. Wang, and S. Sun, "Robust frequency-domain timing offset estimation for DCO-OFDM systems," *IEEE Commun. Lett.*, vol. 26, no. 8, pp. 1603–1607, Jul. 2022.

[9] J. Tan, Z. Wang, Q. Wang, and L. Dai, "Near-optimal low-complexity sequence detection for clipped DCO-OFDM," *IEEE Photon. Technol. Lett.*, vol. 28, no. 3, pp. 233–236, Feb. 2016.

[10] X. Deng, S. Mardanikorani, G. Zhou, and J.-P. M. G. Linnartz, "DC bias for optical OFDM in visible light communications," *IEEE Access*, vol. 7, pp. 98319–98330, 2019.

[11] X. Ling, J. Wang, X. Liang, Z. Ding, and C. Zhao, "Offset and power optimization for DCO-OFDM in visible light communication systems," *IEEE Trans. Signal Process.*, vol. 64, no. 2, pp. 349–363, Jan. 2016.

[12] W. W. Hu, "PAPR reduction in DCO-OFDM visible light communication systems using optimized odd and even sequences combination," *IEEE Photon. J.*, vol. 11, no. 1, Feb. 2019, Art. no. 7901115.

[13] J. Armstrong and A. J. Lowery, "Power efficient optical OFDM," *IET Electron. Lett.*, vol. 42, no. 6, pp. 370–372, Mar. 2006.

[14] A. W. Azim, Y. L. Guennec, M. Chafii, and L. Ros, "Filtered asymmetrically clipped optical-OFDM with index modulation for optical wireless systems," *IEEE Commun. Lett.*, vol. 25, no. 5, pp. 1592–1595, May 2021.

[15] S. Hessien, S. C. Tokgöz, N. Anous, A. Boyacı, M. Abdallah, and K. A. Qaraqe, "Experimental evaluation of OFDM-based underwater visible light communication system," *IEEE Photon. J.*, vol. 10, no. 5, Oct. 2018, Art. no. 7907713.

[16] X. Qian, H. Deng, and H. He, "Joint synchronization and channel estimation of ACO-OFDM systems with simplified transceiver," *IEEE Photon. Technol. Lett.*, vol. 30, no. 4, pp. 383–386, Feb. 2018.

[17] X. Liu, J. Li, Y. Ren, and Z. Huang, "Iterative pairwise maximum likelihood receiver for ACO-OFDM in visible light communications," *IEEE Photon. J.*, vol. 13, no. 2, Apr. 2021, Art. no. 7300107.

[18] S. Feng, Q. Wu, C. Dong, and B. Li, "A spectrum enhanced ACO-OFDM scheme for optical wireless communications," *IEEE Commun. Lett.*, vol. 27, no. 2, pp. 581–585, Feb. 2023.

[19] S. C. J. Lee, S. Randel, F. Breyer, and A. M. J. Koonen, "PAM-DMT for intensity modulated and direct-detection optical communication systems," *IEEE Photon. Technol. Lett.*, vol. 21, no. 23, pp. 1479–1751, Dec. 2009.

[20] N. Huang, J.-B. Wang, J. Wang, C. Pan, H. Wang, and M. Chen, "Receiver design for PAM-DMT in indoor optical wireless links," *IEEE Photon. Technol. Lett.*, vol. 27, no. 2, pp. 161–164, Jan. 2015.

[21] W. W. Hu, "Design of cyclic shifted PAM-DMT signals in HACO-OFDM visible light communication," *IEEE Commun. Lett.*, vol. 24, no. 12, pp. 2834–2838, Dec. 2020.

[22] S. D. Dissanayake and J. Armstrong, "Comparison of ACO-OFDM, DCO-OFDM and ADO-OFDM in IM/DD systems," *J. Lightw. Technol.*, vol. 31, no. 7, pp. 1063–1072, Apr. 2013.

[23] X. Huang, F. Yang, C. Pan, and J. Song, "Advanced ADO-OFDM with adaptive subcarrier assignment and optimized power allocation," *IEEE Wireless Commun. Lett.*, vol. 8, no. 4, pp. 1167–1170, Aug. 2019.

[24] S. K. Lee, T. Y. Chen, and C. C. Lee, "Regarding a pre-distorted ADO-OFDM system as a DCO-OFDM system for visible light communications," *IEEE Access*, vol. 9, pp. 154651–154658, 2021.

[25] R. Bai, R. Jiang, T. Mao, W. Lei, and Z. Wang, "Iterative receiver for ADO-OFDM with near-optimal optical power allocation," *Opt. Commun.*, vol. 387, pp. 350–356, Mar. 2017.

[26] C. He and J. Armstrong, "Clipping noise mitigation in optical OFDM systems," *IEEE Commun. Lett.*, vol. 21, no. 3, pp. 548–551, Mar. 2017.

[27] W. Niu et al., "Neural-network-based nonlinear tomlinson-harashima precoding for bandwidth-limited underwater visible light communication," *J. Lightw. Technol.*, vol. 40, no. 8, pp. 2296–2306, Apr. 2022.